

Role of Dimensionality in Predicting the Spontaneous Behavior of the Brain using the Classical Ising Model and the Ising Model Implemented on the Structural Connectome

Pubuditha M. Abeyasinghe^{1,2*}, Demetrius R. Paula^{1,2}, Sina Khajehabdollahi^{1,2}, Sree Ram Valluri¹, Adrian M. Owen^{2,3}, Andrea Soddu^{1,2*}

1 Department of Physics & Astronomy, Western University, London, ON, Canada

2 The Brain & Mind Institute, Western University, London, ON, Canada

3 Department of Psychology, Western University, London, ON, Canada

* pabeyasi@uwo.ca * asoddu@uwo.ca

There is accumulating evidence that spontaneous fluctuations of the brain are sustained by a structural architecture of axonal fiber bundles. Various models have been employed to investigate this structure-function relationship. In this work, we implemented the Ising model using the number of fibers between each pair of brain regions as input. The output of the Ising model simulations on a structural connectome was then compared with empirical functional connectivity data. A simpler 2-dimensional classical Ising model was used as the baseline model for comparison purpose. Thermodynamic properties, such as the magnetic susceptibility and the specific heat, illustrated a phase transition from an ordered phase to a disordered phase at the critical temperature. Despite the differences between the two models, the lattice Ising model and the Ising model implemented on a structural connectome (the generalized Ising model) exhibited similar patterns of the global properties. To study the behavior of the generalized Ising model around criticality, calculation of the dimensionality and critical exponents was performed for the first time, by introducing a new concept of distance based on structural connectivity. Same value inside the fitting error was found for the dimensionality in both models suggesting similar behavior of the models around criticality.

I. Introduction

The relationship between the spontaneous activity of the brain and its structural fiber distribution is a critical topic in neuroscience. This relationship will allow us to better understand the emergence of complex but flexible dynamics (brain functions) in the brain from its underlying structural network. The structure-function relationship is commonly investigated using two main approaches. First, statistical methods directly compare resting state functional connectivity patterns with the structure. Statistical comparisons lead to important results indicating the presence of a significant correlation between the anatomical fiber distribution and the functional connectivity patterns (Barttfeld et al, 2015, Van Den et al., 2010, Li'egeois R et al., 2015). The other common approach to understand the structure-function relationship of the brain is by using simple mathematical models that could capture the complex dynamics of the brain.

There are several models which have been used to discuss the spontaneous behavior of the brain, including the Neural mass model, the Kuramoto model, and the well-known 2-dimensional (2D) classical Ising model. The Neural mass model and the Kuramoto model have been successful in providing evidence for the existence of a connection between the anatomical structure and the spontaneous fluctuations of the brain as captured by fMRI (David et al., 2004, Honey et al., 2009, Acebro'n et al., 2005, Breakspear et al., 2010, Deco et al., 2009).

The classical Ising model was developed by Ernest Ising (Brush, 1967) to explain the phase transition to ferromagnetic behavior at a critical temperature. It has been used to investigate brain dynamics by (Fraiman et al., 2009). The classical Ising model is a relatively simple model with only one fitting parameter, the temperature of the thermal bath, in which a lattice simulating the regions of a ferromagnet is immersed. Yet, by virtue of its simplicity it has been able to capture the integration and segregation behavior of spontaneous brain function (Fraiman et al., 2009) (for more details of the 2D classical Ising model see APPENDIX A). Blood Oxygen Level Dependent (BOLD) signal is the signal fMRI methods are sensitive to and are a convolved property of neuronal fluctuations in the brain. It is modelled with the Ising model using binary spin states. BOLD signals greater than a threshold will be represented by up spins and less than the threshold will be

represented by down spins with the lattice sites counting the number of brain regions. With this analogy, the 2D classical Ising model was first used by Fraiman to predict the distribution of functional correlations in the brain. They found that the best prediction of the distribution of correlations was obtained from the model at the critical temperature while important deviations were observed for even small changes in temperature from criticality. Successful results of these comparisons have led to further investigations of the model to explain the structure-function relationship of the brain.

In a subsequent work, the 2D classical Ising model was generalized by Marinazzo et al., (Marinazzo et al., 2013) by implementing the model on the structural connectome, in order to match each region of the brain with a corresponding lattice site. Criticality was confirmed for the generalized model and an information transfer was found to be maximum at the critical temperature as well. The generalized Ising model was further studied by Stramaglia et al. by comparing correlation values and transfer entropy between simulated and functional empirical data (Stramaglia et al., 2017). Furthermore, Deco et al. studied an Ising model implemented on the structural connectome and compared with the implementations of the model on artificially created connectomes with different coupling strengths (Deco et al., 2012). They investigated the entropy of the systems as a function of the coupling strength to conclude that the simulated system exhibits rich dynamics similar to the empirical functional connectivity when the structure is integrated as a scale-free network.

In this paper we compared the classical Ising model and the Ising model implemented on the structural connectome with respect to the empirical data demonstrating that both models exhibit similar functional patterns and global properties despite the intrinsic differences. If both models are in the same universality class (same critical exponents), then their similarity would not be surprising. To investigate the cause of their similarities, the critical exponents (explained below as well as in APPENDIX B) of both models were calculated and compared (Landau et al., 2014). If we know the critical exponents of one system in a particular universality class, we can explain any other system in the same universality class, whose microscopic causes could be totally different from the known system. The critical exponents are said to explain the behavior of the system around the

critical temperature. Greek letters, β , γ , α , η and ν are used to represent the critical exponents of magnetizations, susceptibility, specific heat, correlation function (Expert, P. et al., 2011) and correlation length (Fraiman, D. et al., 2012) respectively. These critical exponents together with the dimensionality d follow the scaling relations explained in APPENDIX B.

Dimensionality, together with the other critical exponents, is fundamental to understand the behavior of the system around criticality. Physiological changes of the brain, as for example induced by sleep, could be in fact explained by the model deviating from criticality. Dimensionality of a system has been found to be highly relevant for the system performance also in neural networks (Severino et al., 2016). In their paper, they have concluded that different dynamics can be observed in neural networks with different connectivity patterns coming from different dimensionalities.

For the classical Ising model the dimensionality of the system is given by the number of dimensions of the lattice ($d = 2$ for a square lattice) and there is a well-defined relationship between the number of nearest neighbors in the lattice and the dimensionality (number of nearest neighbors = $2 \cdot \text{dimensionality}$). However, for the generalized Ising model the dimensionality of the system is not evident as for the classical case and in order to be extracted a new concept of distance needed to be introduced.

The key components of the steps carried out are summarized in Fig. 1. The organization of the paper is as follows. In the next section, we will introduce the methodology of calculating and comparing properties of the empirical functional connectivity with the ones generated from the numerical simulations of the classical Ising model and the generalized Ising model. Then we will explain the procedure we followed to calculate the critical exponents and the dimensionality of the models. Next, we will explain the main findings of the work that was carried out, which will be followed by discussion and conclusions.

II. Materials and Methods

A. Acquisition & Preprocessing of Data

1. Subjects

A set of sixty-six healthy subjects, between 22 – 35 years old, were studied during wakefulness. Informed consent to participate in the study was obtained from every subject.

2. Ethics Statement

The Ethics Committee of the Washington University and the University of Minnesota approved the study.

3. Acquisition & Preprocessing of Data

Structural and functional data were acquired at the Washington University - University of Minnesota Consortium of the Human Connectome Project (WU-Minn HCP). Details about the data acquisition and preprocessing can be found here (Glasser, Mathew F. et al., 2013, Jenkinson, Mark, et al. , 2012, Fischl B. 2012, Jenkinson M et al., 2002, Glasser MF et al., 2011, Van Essen DC et al., 2012, Andersson JL et al., 2003, Andersson JL et al., 2015, Andersson JL et al., 2015). Parcellation of the data was performed, using FSL, Freesurfer and MRTrix software with 84 individually labeled regions (list of the labels are presented in APPENDIX C). Extraction of the structural connectivity matrix (J_{ij}) was performed using the MRTrix software.

B. 2D Ising model and the Generalized Ising Model

1. Computer Simulations:

An instance of the 2D Ising model is built starting with a random spin configuration on a square lattice of size $L \times L$ ($= 9 \times 9$) which is in contact with a thermal bath of temperature T . For comparison purposes, a square lattice Ising model with a 9×9 lattice size was chosen, as it gives 81 spin sites (that is the closest number of sites to 84 we can acquire using a square lattice). For the generalized Ising model, a 1×84 array of random spins was used. Each spin can be in only one of two spin states (either up (+1) or down (-1)). The energy of this spin configuration, in the absence of an external magnetic field is given by;

$$E = - \sum_{i,j=1}^N J_{ij} S_i S_j \quad (I)$$

where J_{ij} is the coupling between i^{th} and j^{th} region, s_i and s_j represent the spins of the i^{th} and j^{th} region respectively and $N = L \times L$. A matrix representing the coupling J_{ij} for the 2D Ising model has been created to encode nearest neighbor coupling with a coupling strength of one (Fraiman et al., 2009). In contrast, another matrix representation of coupling J_{ij} for the generalized Ising model has been created using the connectivity matrix which was built from the Diffusion Tensor Image (DTI) acquisition. This matrix contains the number of fiber tracts between each pair of region in the connectome which is being used to define the coupling strength. For the simulations of the model we normalized the average structural connectivity matrix (average over 66 subjects) such that the matrix elements will be between 0 and 1.

A Metropolis Monte Carlo algorithm (Metropolis et al., 1953, Gould et al., 1988) was used to simulate the system at each temperature. Metropolis Monte Carlo algorithm allows to generate an equilibrium spin configuration starting from a random spin configuration for each temperature (more details can be found in APPENDIX A). From the final output of the simulations, the correlation between the time evolutions of spins for each temperature was calculated using Eq. II,

$$corr_{ij} = \frac{\langle s_i(t) \times s_j(t) \rangle - \langle s_i(t) \rangle \langle s_j(t) \rangle}{\sigma_{s_i(t)} \times \sigma_{s_j(t)}} \quad (II)$$

where s_i and s_j stands for the spins of i^{th} and j^{th} regions, $\sigma_{s_i(t)}^2 = \langle s_i^2(t) \rangle - \langle s_i(t) \rangle^2$ and $\langle . \rangle$ is for the average over time.

Using this procedure, the correlations were generated by each model as a function of temperature. Afterwards, this procedure was repeated for both models to generate ten sets of data for each, always starting with a random spin configuration. Generating ten independent simulations further ensures that the Metropolis algorithm explores a variety of initial conditions and therefore increases the (statistical) accuracy of the results. MATLAB (<https://www.mathworks.com/>) was used for the computer simulations and analysis whereas RStudio (<https://www.rstudio.com/>) was used to generate graphs.

C. Analysis

1. Preliminary Analysis

Analysis was performed over the average of ten data sets for both models. The thermodynamic properties were plotted as functions of temperature for the two models to obtain the critical temperature (Fig. 2).

The critical temperature can be obtained by locating the temperature which maximizes the magnetic susceptibility of the system (Eq. III where χ is the magnetic susceptibility, T is the temperature and M is the magnetization) (Landau et al., 2014).

$$\chi = \frac{1}{T} [\langle M^2 \rangle - \langle M \rangle^2] \quad (\text{III})$$

The empirical functional correlation matrix which is built by averaging the correlation matrices across the 66 healthy subjects was compared with the simulated correlation matrices (Fig. 3) for further analysis. Additionally, the distribution of the correlation for the simulated data as well as for the empirical data was plotted in Fig. 4.

Next, the distance between the simulated correlation distributions and the empirical correlation distribution was calculated as a function of temperature and presented in APPENDIX D - I. The distance between the empirical and simulated correlation distributions is quantified using the Kolmogrove-Smirnov test (KS test) statistic (Massey Jr et al., 1951). To calculate the KS test statistic, empirical and the simulated correlations were plotted as cumulative plots in the same graph. Next, the maximum distance between these two plots was calculated. Temperatures which minimize this maximum distance (T_{min}) has been obtained for individual simulations. Distribution of T_{min} and T_c for the generalized Ising model is presented in Fig. 5.

In order to calculate the global degree as a function of threshold, correlations were separated into positive and negative correlations. Then the global degree was calculated for the negative and positive thresholds separately for the 2D classical Ising model and the generalized Ising model and plotted in Fig. 6 together with the global degree of the empirical data (Rubinov et al., 2010). Taking the individual node degree into consideration,

connectivity graphs are plotted for the generalized Ising model at four different temperatures and been compared with the graph of the empirical data (Fig. 7)

2. Analyzing the behavior at the criticality using the critical exponents

The critical exponents and the dimensionality were calculated for the two models by following the procedure below. First, the critical exponents related to magnetization, susceptibility and specific heat were calculated by fitting Eq. 1- 5 (in APPENDIX B) to the respective plots in Fig. 2. To find η and ν , following procedure was used:

Correlation function: First, a set of distances for both models were defined using the respective connectivity matrices. For the classical Ising model, the distances were the integers from 1 to 8, since the initial configuration was a 9 x 9 2D lattice. However, for the generalized Ising model the distance between two regions is defined as the reciprocal of the normalized number of fibers between the two regions ($d_{ij} = 1/J_{ij}$). We binned the continuous distances to create a set of discrete groups. Then the correlation values between pairs at the same distance were averaged to get the average correlation as a function of distance. This calculation was performed for each temperature (Fig. 8). By fitting Eq. 8 (APPENDIX B) to the plot of correlation function versus the distance at the critical temperature, η was calculated. By subsequently using Eq. 7 to fit the correlation function at the critical temperature, a numerical value for the power of the denominator ($= d - 2 + \eta$) was then obtained. Using this fitted value and the calculated η at T_c the dimensionality of the classical Ising model as well as the generalized Ising model was finally extracted.

Correlation length: Correlation length at each temperature was calculated by fitting Eq. 6 (APPENDIX B) to the correlation function versus the distance at each temperature. The correlation length was plotted as a function of temperature and fitted with Eq. 9 and 10 (APPENDIX B) to find ν (Fig. 8).

III. Results

1. Preliminary Analysis

The mean values of critical, sub-critical and super critical temperatures over the ten independent trials were obtained using the susceptibility plots in Fig. 2 and are reported in

Table I together with their standard deviations. The critical temperature value of the 2D Ising model agree with the critical temperature described in (Witthauer et al., 2007) for the lattice size $L = 9$. In the generalized Ising model, the phase transition occurs at a lower temperature than that of the classical Ising model. Correlations for four different temperatures are presented in Fig. 3. At T_c the spatial pattern of the correlations in the generalized Ising model hold a similar spatial pattern to that of the empirical data. Distributions of the correlations for the selected four temperatures are plotted in Fig. 4 along with the empirical data. For the classical Ising model correlation distributions showed difference between the empirical distribution and the simulated one at criticality, even if the critical temperature T_c or the slightly different value T_{min} gave a much better prediction with respect to sub or supercritical behavior. For the generalized Ising model the distribution of correlations at T_c and T_{min} and the distribution of correlations for the empirical data were not significantly different ($p = 0.98$) while the distributions at sub and supercritical temperatures were quite distant from the empirical distribution.

According to Fig. 5, the variation of T_c (and T_{min}) is resulted due to the randomness of the initial spin configuration in the simulations. To illustrate the inter-subject variance of T_c (and T_{min}), distributions of T_c (and T_{min}) are presented in APENDIX D - (II). A two sample t-test was performed to compare the T_{min} values with the T_c values in individual simulations. Results of the t-test together with Fig. 5 concluded that T_{min} and T_c are significantly different for the generalized Ising model ($p < 0.001$) but not significantly different for the 2D Ising model (with $p = 0.4$).

Graph Theoretical Analysis

In Fig. 6, the global degree of the graphs was plotted as a function of negative and positive thresholds for both models. As observed in Fig. 4 there are no negative correlations at T_c or at T_{min} for the classical Ising model. Therefore, in Fig. 6 the degree cannot be plotted for the negative thresholds at T_c and at T_{min} for the classical Ising model. Fig. 7 represents the functional connectivity graphs for the data obtained from the generalized Ising model simulations at sub-critical, critical, super-critical temperatures and T_{min} along with the connectivity graph of the empirical data. In these graphs, each point represents a brain

region. It is evident that the connectivity in the network grows as the temperature goes from $T < T_c$ to T_c and again reduced from T_c to $T > T_c$, and shows similar patterns for T_c and T_{min} .

Analyzing the behavior at the criticality using the critical exponents

Fig. 8 represents the correlation function and the correlation length plotted for the two models. These two plots were used to find the critical exponent η and the dimensionality 'd' of the models. The calculation of dimensionality for the classical Ising model confirmed the expected value of 2 (since we chose the square lattice Ising model in two dimensions) giving the value of 1.93 ± 0.59 . The dimensionality of the generalized Ising model was calculated for the first time giving a value of 1.92 ± 0.12 and proven equal to the classical Ising model value inside the fitting error. All the other critical exponents are reported in Table II together with the dimensionality for both models.

IV. Discussion

The square lattice Ising model has been used in neuroscience to study brain functionality. Fraiman et al. showed that the distribution of correlations at T_c in the 2D classical Ising model has noticeable similarities to the distribution of correlations of the empirical data, even in the absence of information from the structural architecture of the brain (Fraiman et al., 2009). Their conclusion together with several other studies supported the assumption of the presence of critical behavior in the brain network (Marinazzo et al., 2013, Stramaglia et al., 2017, Deco et al., 2012).

In this paper, as the first step we compared simulations of a 2D Ising model with those of the generalized Ising model by looking at the distributions of correlation values. The fact that for both models the mean of the correlation distribution values at the critical temperature is larger than the mean of the correlation distribution at sub-critical or super-critical temperatures is a well known prediction of the Ising model in the classical version and was confirmed by our results for the generalized model. Correlation between the i^{th} and the j^{th} regions can be calculated using Eq. (IV) (where r_{ij} is the distance between region i and j , ξ is the correlation length, d is the dimensionality and η is the critical exponent of the correlation function), and is clearly shown from Fig. 8.

$$corr_{ij} = \frac{\exp(-\frac{r_{ij}}{\xi})}{r^{d-2+\eta}} \quad (IV)$$

At the critical temperature, because the correlation length (ξ) goes to infinity (in the infinite lattice size limit), the correlation will have a power law decay with the distance. On the contrary, at any other temperature, ξ will be finite and the correlation will have a combined exponential and power law decay. Therefore, outside of criticality correlation will drop faster with distance resulting in a lower average correlation value. For finite lattice size the difference between the mean of the distribution at criticality and outside criticality will be reduced with respect to the infinite lattice size limit.

In the generalized Ising model, the introduction of the coupling from the structural connectivity of the brain provided a one to one relationship between the brain regions and the lattice sites. Each lattice site was connected with every other site with a given weight which was obtained from DTI as opposed to the 2D classical Ising model. One objective was to investigate behavior at the critical temperature with respect to these changes in the model. When the structure is introduced, we observed a shift in the critical temperature from 2.5 to 1.4. An illustration of this change as a function of sparsity of the structural connectivity matrix is presented in APPENDIX D – (III). We can conclude that the critical temperature depends not only on the size of the matrix but also on the sparsity of the connectivity matrix.

The temperature which minimizes the distance between the distributions of correlation (T_{min}) was significantly different from T_c for the generalized Ising model but not for the 2D classical Ising model. Global degree plotted as a function of the temperature (APPENDIX D – (IV)) was maximized at a temperature which is not different from T_{min} . This fact suggests the usage of graph properties to extract T_{min} of the Ising model, either in the classical or generalized version as done by looking for the maximum of susceptibility. Fig. 9 represents the possibility of finding a relationship between the graph properties and the thermodynamic properties of the Ising model. As the theory implies, the specific heat and the susceptibility measure the variation of energy and magnetization with temperature respectively. This was captured by calculating the cumulative integral of the specific heat and susceptibility of the generalized Ising model. Following the same procedure, the

cumulative integral of the global degree was calculated, which resulted in the plot on the right-hand corner in the top panel of Fig. 9. The new plotted quantity follows a similar behavior as the energy with temperature and could be linked to a fundamental property of graph theory.

Similar properties around criticality for both models justified the use of the same fitting functions, even if we needed to introduce a concept of distance for the generalized version in order to extract the correlation length. In fact as shown in Fig. 8 the behavior of the correlation vs distance for the generalized Ising model is well fitted by the same function as the classical model.

Having the same dimensionality can explain the observed similarities in global behavior of the two Ising models around the critical temperature such as the correlation values and global degree. Studying the behavior around criticality for complex systems like the Ising model which shows a phase transition, could be extremely important and performed with a similar strategy as the one followed in this paper by introducing an artificial concept of distance.

As the critical exponents (in Table II) are different for the two models, it cannot be concluded that these models belong to the same universality class. The fact that the global properties of the models still followed a similar pattern is due to the fact that our calculated properties all depend on the correlation values which are controlled by the dimensionality d (equal in the two models) and the critical exponent η (0.34 for classical and 0.46 for generalized) (APPENDIX B, Eq. 6).

Our findings for the generalized Ising model could be of relevance to study for example the brain function of patients who suffer severe brain injury with disorders of consciousness in which usually both structural and functional connectivity are highly affected. Furthermore, for future studies, it will be highly relevant to see how the properties of the generalized Ising model change with respect to the size of the lattice. This would mean using different parcellation schemes, different size of the system, which is contrary to the classical Ising model will also result in the change of the structural connectivity matrix (J_{ij}) that will depend on the parcellation scheme used.

V. Conclusion

Extending the 2D classical Ising model towards the generalized Ising model further permits to fit the empirical functional connectivity patterns. The introduction of structural data from the brain as an input into the Ising model gives the best fit to functional data at T_{\min} which is significantly different from T_c in the direction of the subcritical regime but not far from criticality. Since the critical exponents of the models are different it cannot be concluded that these two models belong to the same universality class. However, similarities observed in the global properties between the two models can be explained by the fact that they have the same dimensionality. Studying the behavior of the system around criticality could be used to better understand changes in spontaneous brain activity from the awake condition as observed in physiological states like sleep or as in pharmacologically induced conditions like under anesthetics.

Acknowledgement

We would like to acknowledge the Human Connectome Project (HCP) for providing the data. In particular, the data were provided by the HCP, WU-Minn Consortium (Principal Investigators: David Van Essen and Kamil Ugurbil; 1U54MH091657) funded by the 16 NIH Institutes and Centers that support the NIH Blueprint for Neuroscience Research; and by the McDonnell Center for Systems Neuroscience at Washington University. Furthermore, we would like to extend the acknowledgement to Marco Aiello and Carlo Cavaliere from NAPLAB, Naples (Italy) for performing the parcellation of the preprocessed HCP data and for the extraction of the structural connectivity matrix from the DTI data.

Author Disclosure Statement

No competing financial interests exist

References

- Acebro'n JA, Bonilla LL, Vicente CJP, Ritort F, Spigler R. The Kuramoto model: A simple paradigm for synchronization phenomena. *Reviews of modern physics*. 2005;77(1):137.
- Andersson JL, Skare S, and Ashburner J. (2003). How to correct susceptibility distortions in spin-echo echo-planar images: application to diffusion tensor imaging. *NeuroImage*. 20(2):870-888.
- Andersson JL, Sotiropoulos SN (2015). Non-parametric representation and prediction of single- and multi-shell diffusion-weighted MRI data using Gaussian processes. *Neuroimage*. 2015 Nov 15;122:166-76.
- Andersson JL, Sotiropoulos SN (2015). An integrated approach to correction for off-resonance effects and subject movement in diffusion MR imaging. *Neuroimage*. 2015 Oct 16. pii: S1053-8119(15)00920-9.
- Barttfeld P, Uhrig L, Sitt JD, Sigman M, Jarraya B, Dehaene S. Signature of consciousness in the dynamics of resting-state brain activity. *Proceedings of the National Academy of Sciences*. 2015;112(3):887–892.
- Breakspear M, Heitmann S, Daffertshofer A. Generative models of cortical oscillations: neurobiological implications of the Kuramoto model. *Frontiers in human neuroscience*. 2010;4:190.
- Brush SG. History of the Lenz-Ising model. *Reviews of modern physics*. 1967;39(4):883.
- Cammoun L, Gigandet X, Meskaldji D, Thiran JP, Sporns O, Do KQ, et al. Mapping the human connectome at multiple scales with diffusion spectrum MRI. *Journal of neuroscience methods*. 2012;203(2):386–397.
- Daducci A, Gerhard S, Griffa A, Lemkaddem A, Cammoun L, Gigandet X, et al. The connectome mapper: an open-source processing pipeline to map connectomes with MRI. *PloS one*. 2012;7(12):e48121.

- Damoiseaux J, Rombouts S, Barkhof F, Scheltens P, Stam C, Smith SM, et al. Consistent resting-state networks across healthy subjects. *Proceedings of the national academy of sciences*. 2006;103(37):13848–13853.
- David O, Cosmelli D, Friston KJ. Evaluation of different measures of functional connectivity using a neural mass model. *Neuroimage*. 2004;21(2):659–673.
- De Luca M, Beckmann C, De Stefano N, Matthews P, Smith SM. fMRI resting state networks define distinct modes of long-distance interactions in the human brain. *Neuroimage*. 2006;29(4):1359–1367.
- Deco G, Jirsa V, McIntosh AR, Sporns O, Kořtter R. Key role of coupling, delay, and noise in resting brain fluctuations. *Proceedings of the National Academy of Sciences*. 2009;106(25):10302–10307.
- Deco, Gustavo, Mario Senden, and Viktor Jirsa. "How anatomy shapes dynamics: a semi-analytical study of the brain at rest by a simple spin model." *Frontiers in computational neuroscience* 6 (2012): 68.
- Demertzi, Athena, et al. "Multiple fMRI system-level baseline connectivity is disrupted in patients with consciousness alterations." *Cortex* 52 (2014): 35-46
- Expert, Paul, et al. "Self-similar correlation function in brain resting-state functional magnetic resonance imaging." *Journal of The Royal Society Interface* 8.57 (2011): 472-479.
- Fraiman, D., & Chialvo, D. R. (2012). What kind of noise is brain noise: anomalous scaling behavior of the resting brain activity fluctuations. *Frontiers in physiology*, 3.
- Fischl B. (2012). FreeSurfer. *NeuroImage*, 62:774-781.
- Gerhard S, Daducci A, Lemkaddem A, Meuli R, Thiran JP, Hagmann P. The connectome viewer toolkit: an open source framework to manage, analyze, and visualize connectomes. *Frontiers in neuroinformatics*. 2011;5.

- Glasser, Matthew F., et al. "The minimal preprocessing pipelines for the Human Connectome Project." *Neuroimage* 80 (2013): 105-124.
- Glasser MF, and Van Essen DC. (2011). Mapping human cortical areas in vivo based on myelin content as revealed by T1- and T2-weighted MRI. *J Neurosci.* 31:11597-11616
- Gorgolewski K, Burns CD, Madison C, Clark D, Halchenko YO, Waskom ML, et al. Nipype: a flexible, lightweight and extensible neuroimaging data processing framework in python. *Frontiers in neuroinformatics.* 2011;5.
- Gould H, Tobochnik J, Christian W, Ayars E. An introduction to computer simulation methods: applications to physical systems. vol. 1. Addison-Wesley Reading; 1988.
- Honey C, Sporns O, Cammoun L, Gigandet X, Thiran JP, Meuli R, et al. Predicting human resting-state functional connectivity from structural connectivity. *Proceedings of the National Academy of Sciences.* 2009;106(6):2035–2040.
- Jenkinson, Mark, et al. "Fsl." *Neuroimage* 62.2 (2012): 782-790.
- Jenkinson M, Bannister PR, Brady JM, and Smith SM. (2002). Improved optimisation for the robust and accurate linear registration and motion correction of brain images. *NeuroImage* 17(2):825-841.
- Landau, David P., and Kurt Binder. *A guide to Monte Carlo simulations in statistical physics.* Cambridge university press, 2014.
- Liégeois R, Ziegler E, Phillips C, Geurts P, Go´mez F, Bahri MA, et al. Cerebral functional connectivity periodically (de) synchronizes with anatomical constraints. *Brain Structure and Function.* 2015; p. 1–13.
- Marinazzo D, Pellicoro M, Wu GR, Angelini L, Cortes JM, Stramaglia S. Information transfer of an Ising model on a brain network. *BMC Neuroscience.* 2013;14(1):1.
- Massey Jr, Frank J. "The Kolmogorov-Smirnov test for goodness of fit." *Journal of the American statistical Association* 46.253 (1951): 68-78.

- Metropolis N, Rosenbluth AW, Rosenbluth MN, Teller AH, Teller E. Equation of state calculations by fast computing machines. *The journal of chemical physics*. 1953;21(6):1087–1092.
- Penny WD, Friston KJ, Ashburner JT, Kiebel SJ, Nichols TE. *Statistical parametric mapping: the analysis of functional brain images*. Academic press; 2011.
- Ribeiro de Paula, Demetrius, et al. "A method for independent component graph analysis of resting-state fMRI." *Brain and Behavior* (2017).
- Rubinov M, Sporns O. Complex network measures of brain connectivity: uses and interpretations. *Neuroimage*. 2010;52(3):1059–1069.
- Severino, Francesco Paolo Ulloa, et al. "The role of dimensionality in neuronal network dynamics." *Scientific Reports* 6 (2016).
- Stramaglia, S., Pellicoro, M., Angelini, L., Amico, E., Aerts, H., Cortés, J.M., Laureys, S. and Marinazzo, D., 2017. Ising model with conserved magnetization on the human connectome: Implications on the relation structure-function in wakefulness and anesthesia. *Chaos: An Interdisciplinary Journal of Nonlinear Science*, 27(4), p.047407.
- Tournier JD, Calamante F, Gadian DG, Connelly A. Direct estimation of the fiber orientation density function from diffusion-weighted MRI data using spherical deconvolution. *NeuroImage*. 2004;23(3):1176–1185.
- Van Den Heuvel MP, Pol HEH. Exploring the brain network: a review on resting-state fMRI functional connectivity. *European Neuropsychopharmacology*. 2010;20(8):519–534.
- van den Heuvel, Martijn P., and Olaf Sporns. "Network hubs in the human brain." *Trends in cognitive sciences* 17.12 (2013): 683-696.
- Van Essen DC, Glasser MF, Dierker DL, Harwell J, and Coalson T. (2012). Parcellations and hemispheric asymmetries of human cerebral cortex analyzed on surface-based atlases. *Cereb. Cortex* 22:2241-2262
- Witthauer L, Dieterle M. The phase transition of the 2D-Ising model; 2007.

TABLE I. Sub-critical, critical, super-critical temperatures and T_{min} of the generalized Ising model and the 2D classical Ising model

Model	$T < T_c$	$T = T_{min}$	$T = T_c$	$T > T_c$
Generalized Ising model	0.78 ± 0.02	1.21 ± 0.04	1.39 ± 0.02	1.98 ± 0.02
Classical Ising model	1.55 ± 0.10	2.53 ± 0.20	2.55 ± 0.10	3.55 ± 0.10

TABLE II. Critical exponents and the dimensionality of the 2D classical Ising model and the generalized Ising model

Critical exponent	2D Classical Ising model	Generalized Ising model
α (Specific heat)	1.49 ± 0.02	0.81 ± 0.01
β (Magnetization)	0.14 ± 0.01	0.21 ± 0.01
γ (Susceptibility)	0.61 ± 0.01	0.53 ± 0.01
η (Correlation function)	0.34 ± 0.01	0.46 ± 0.01
ν (Correlation length)	0.30 ± 0.01	0.63 ± 0.02
d (Dimensionality)	1.93 ± 0.59	1.92 ± 0.12

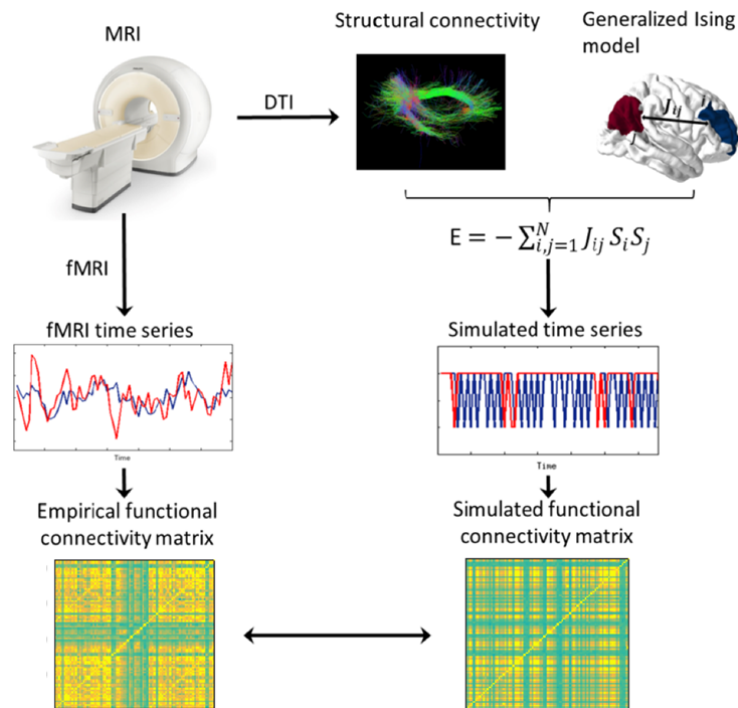


FIG. 1. Summarized representation of the analysis carried out. We obtained the structural and functional data separately from brain imaging techniques. Then, the structural connectivity was used as the input of the generalized Ising model. Using this input, the generalized Ising model was simulated for different temperatures and each time the output was compared with the empirical functional data obtained from fMRI

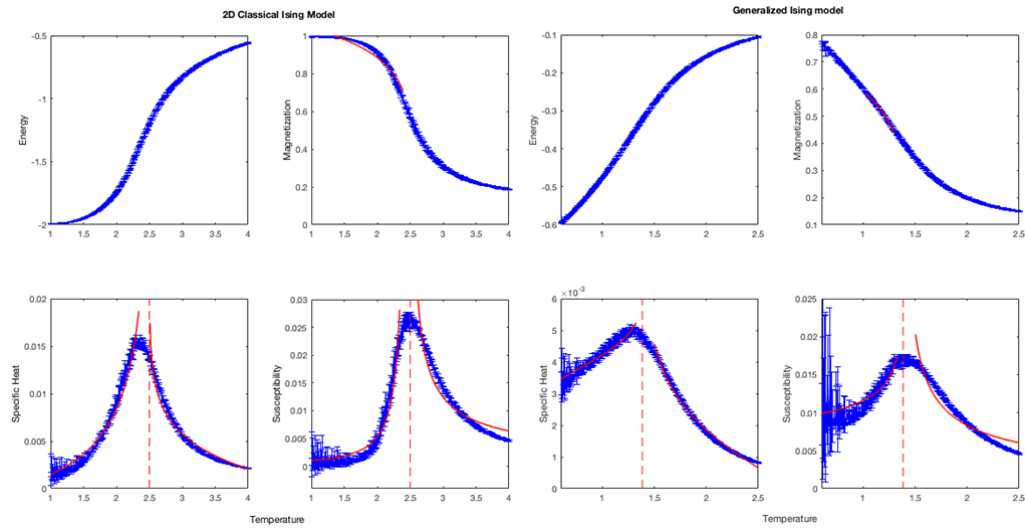


FIG. 2. Thermodynamic properties of the 2D classical Ising model with 9×9 lattice size and the generalized Ising model as a function of temperature. Red dashed line indicates the critical temperature and the red solid lines represents the plots after fitting the given equations to calculate the critical exponents.

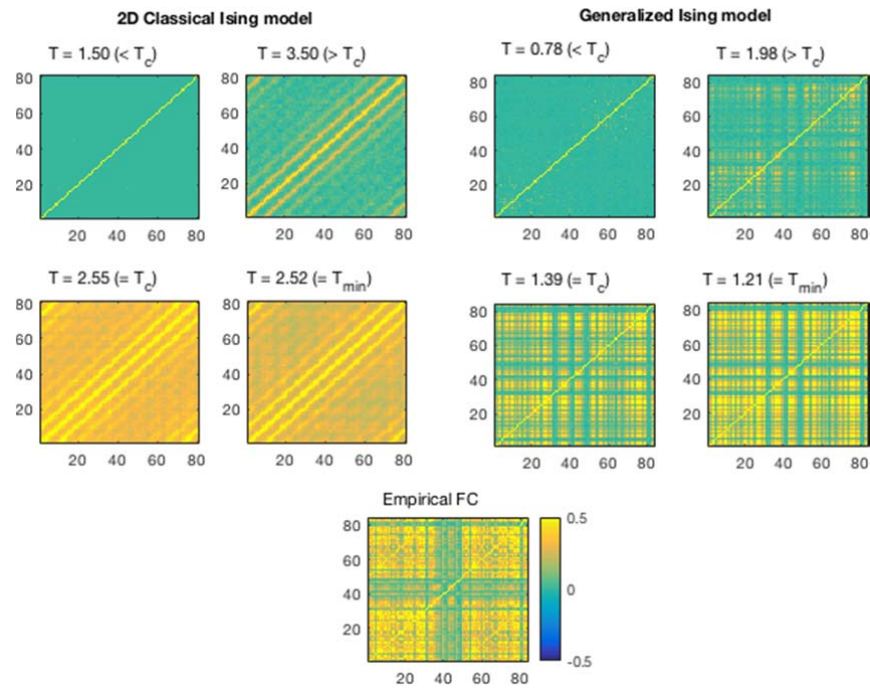


FIG. 3. Correlation at four different temperatures for the classical Ising model and the generalized Ising model with the correlation of the empirical data.

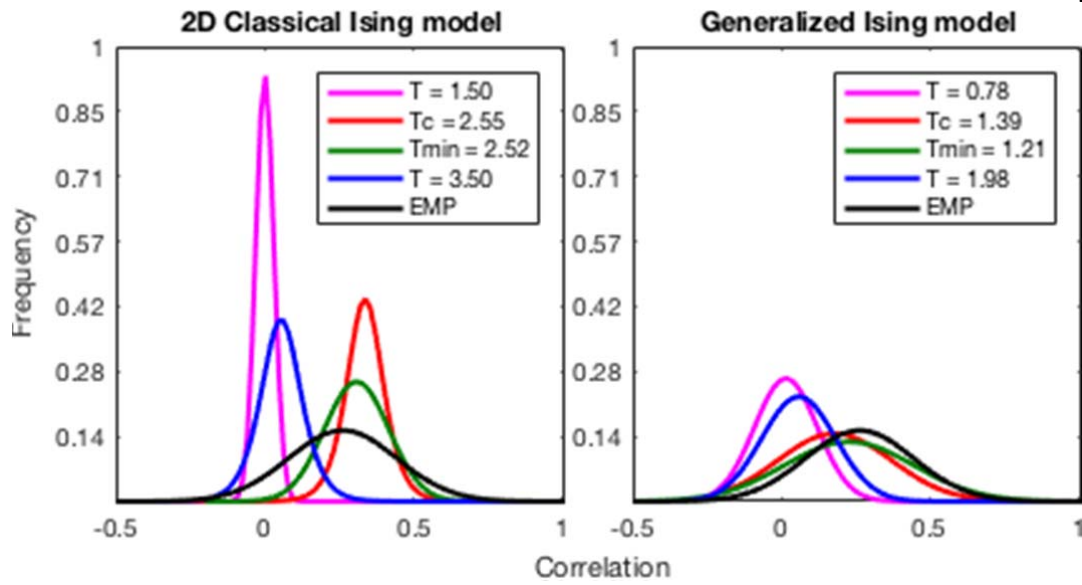


FIG. 4. Distribution of the correlation at four different temperatures for the classical Ising model and the generalized Ising model with the distribution of correlation of the empirical data.

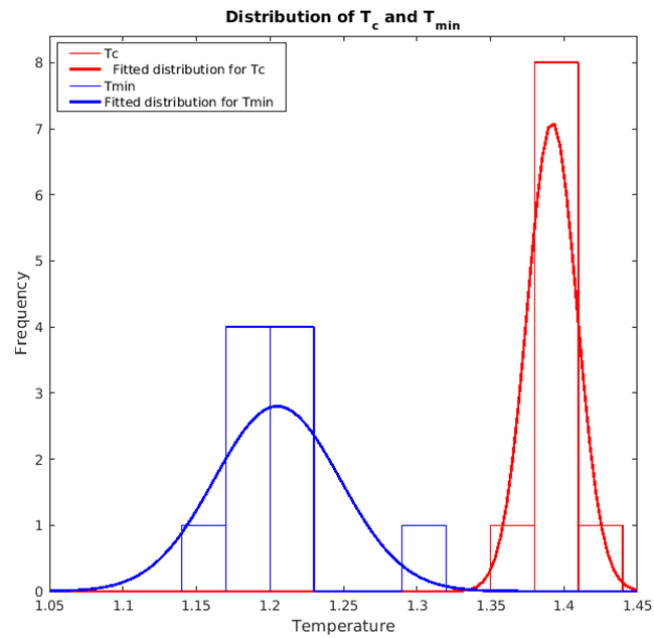


FIG. 5. Histogram of T_c and T_{min} together with the fitted distributions for the generalized Ising model in ten independent simulations

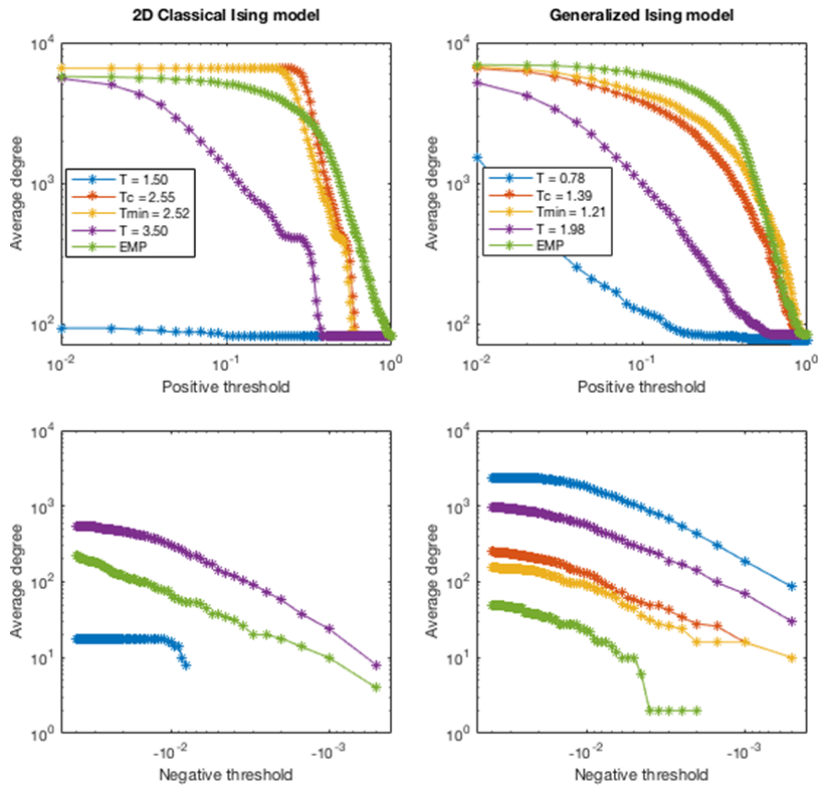


FIG. 6. Average degree as a function of positive and negative thresholds for the classical Ising model and the Generalized Ising model together with the average degree of the empirical correlation network.

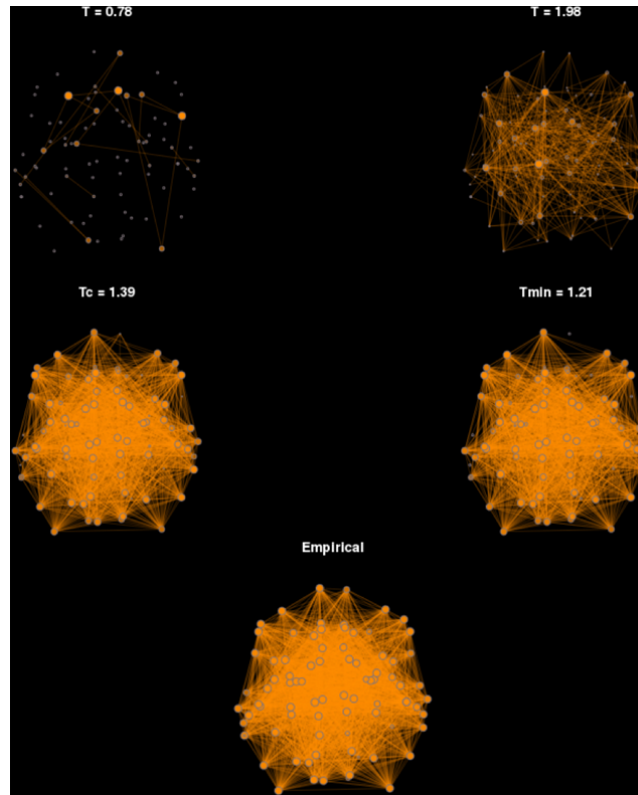


FIG 7. Connectivity graphs for the generalized Ising model for four temperatures, and the connectivity graph of the empirical network. The size of the nodes represents the degree such that larger the size, higher the degree.

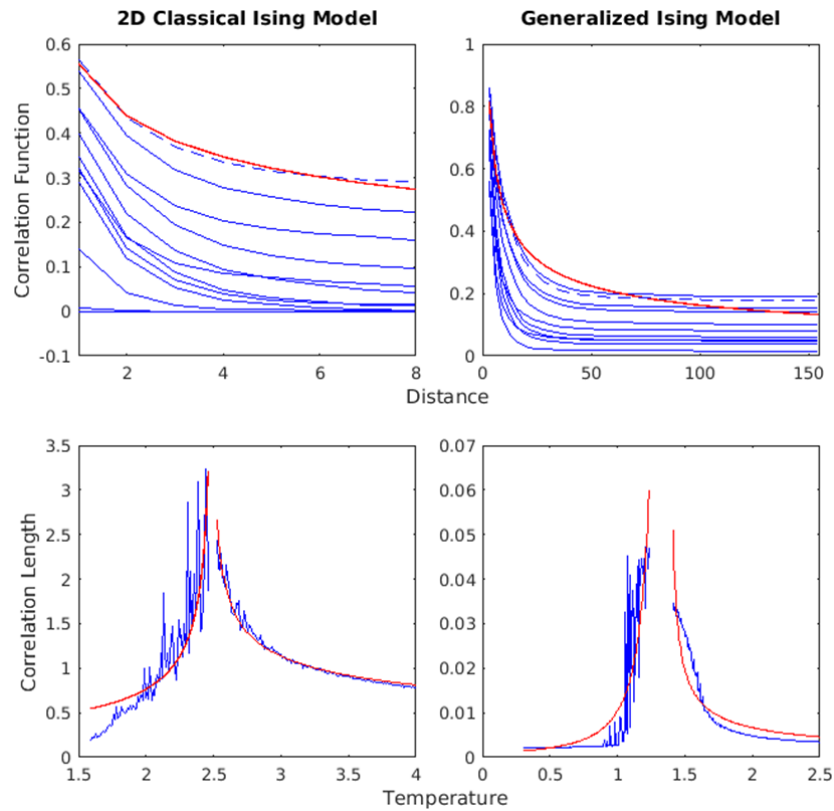


FIG. 8. Correlation function versus distance and correlation length versus temperature for the 2D classical Ising model and the generalized Ising model. Red solid line represents plots after fitting the given equations (APPENDIX B). In the top panel, the dashed line represents the correlation function at the critical temperature.

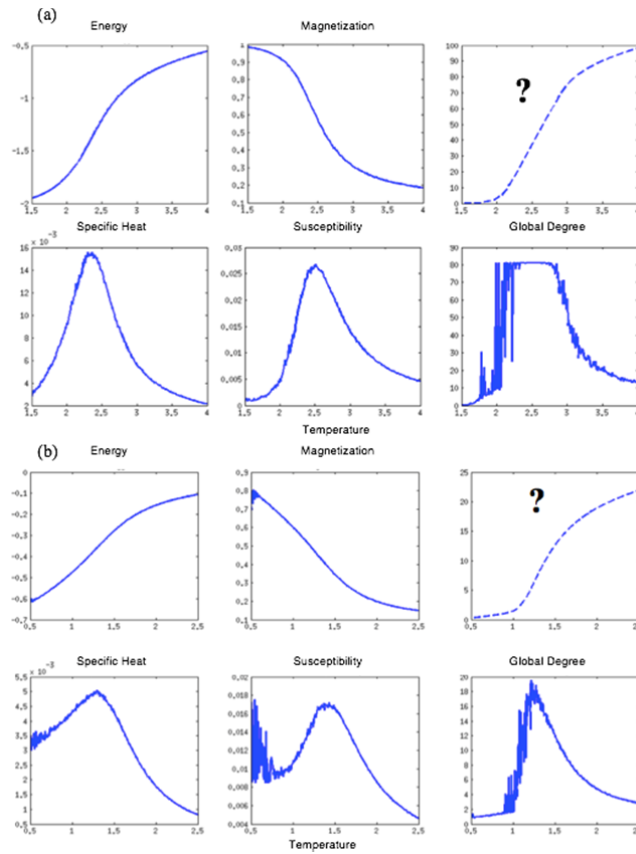


FIG. 9. Energy, Specific Heat, Magnetization, Susceptibility, Degree and the cumulative degree of (a) the generalized Ising model, (b) the 2D classical Ising model as a function of temperature.

APPENDIX

APPENDIX A: 2D CLASSICAL ISING MODEL

APPENDIX A: 2D Classical Ising Model

A detailed explanation of the 2D classical Ising model is given in this Online Resource.

The classical Ising model was introduced by Wilhelm Lenz in 1920. The 2D Ising model (in the absence of an external magnetic field) was solved by Onsager in 1944 (Brush, 1967). It was introduced to explain the interactions of magnetic spins mathematically. The physical system (a magnet) is represented by a lattice configuration in the Ising model. Each lattice site has a spin 's' which could take only two possible values, either up (+1) or down (-1) (Figure 1). Thus, it is a collection of +1 and -1s representing the spins. This configuration is kept in a thermal bath of temperature T. Interactions between the spins are always influenced by this temperature and allow the system to reach an equilibrium energy state while resulting in different equilibrium spin configurations with different properties at different temperatures.

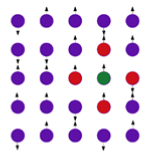


Fig. 1 Representation of a 2D lattice arrangement. Each lattice site has a spin, either up or down. The nearest neighbours of the lattice site in green are represented in red

The energy of this spin system at any state x in the absence of an external magnetic field can be calculated using Equation 1:

$$E(x) = -J \sum_{i,j=\text{nn}(i)}^N s_i s_j \quad (1)$$

where J is the coupling constant, s_i and s_j represent the spins of the i^{th} and j^{th} site respectively, and N is the size of the lattice. For the calculation of energy in the 2D Ising model, only the nearest neighbour interactions are considered together with equal coupling ($J = 1$). The probability of finding the system in the state x

with energy $E(x)$ is given by Equation 2:

$$P(x) = \frac{1}{Z} e^{-\frac{E(x)}{k_B T}} \quad (2)$$

where k_B is the Boltzmann constant, T is the temperature of the heat bath and Z is the partition function. Equation 3 illustrates the partition function of the system which describes the statistical properties of the spin system in thermodynamic equilibrium. The summation is over all possible 2^N spin configurations.

$$Z = \sum_{\{x\}} e^{-\frac{E(x)}{k_B T}} \quad (3)$$

At equilibrium, thermodynamic properties such as magnetization, magnetic susceptibility and the specific heat of the system can be calculated using Equations 4, 5 and 6 respectively where s_i is the spin of the i^{th} spin site. Magnetization simply is an order parameter which explains the state of the spin system, either an ordered state or a disordered state. Magnetic susceptibility is the derivative of magnetization which captures the changes of magnetization. This is used to identify the critical temperature of the spin system by noting the temperature which maximizes the susceptibility (or the temperature which gives the highest variation of magnetization). Specific heat tells us how much does the energy of the spin system changes with changing temperature.

$$M = \frac{1}{N} \left| \sum_{i=1}^N s_i \right| \quad (4)$$

$$\chi = \frac{1}{T} [(M^2) - \langle M \rangle^2] \quad (5)$$

$$C_v = \frac{1}{T^2} [(E^2) - \langle E \rangle^2] \quad (6)$$

When a 2D lattice configuration is considered, there are two extreme equilibrium configurations of spins it can hold, one for lower temperatures (sub-critical) and the other one for higher temperatures (super-critical). When the temperature is very low, all the spins prefer to be aligned along the same direction, with very large clusters of the same spin, either up or down (ordered) resulting in high magnetization even in the absence of an external magnetic field (Figure 2 (a)). In

2

the other end, when the temperature is very high, the spins are a mixture of up spins as well as down spins (disordered) without any order which will result in zero magnetization (Figure 2 (c)). In between these two extremes, there exists a critical temperature (T_c) (Das et al. 2014) where the system exhibits transition from ordered phase to the disordered phase (Figure 2 (b)). As the figure illustrates, at this temperature there is a mixture of ordered spins as well as disordered spins. Additionally, the system acquires its maximum susceptibility or the maximum change in magnetization at T_c . Even a single spin flip can change the entire system (Chialvo, 2010), and the perturbation introduced by a single spin flip can spread over the entire system rapidly. Therefore, with different temperatures of the heat bath, the system could exhibit completely different properties (Brush, 1967) which depend only on the temperature of the system.

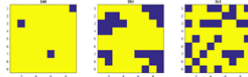


Fig. 2 Representation of the equilibrium spin configuration for (a) $T < T_c$, (b) $T = T_c$ and (c) $T > T_c$ for a two-dimensional lattice arrangement. Yellow color is for the up spins (+1) and blue color is for the down spins (-1)

To impose the dynamics to the classical Ising model, the Metropolis Monte Carlo algorithm is used. The Metropolis algorithm involves the construction of a new state based on the current state of the system with a transition probability. It is used in the Ising model to find the equilibrium energy state starting from a random spin configuration for a constant temperature (Landau and Binder, 2014). This algorithm is used in the classical Ising model with the periodic boundary conditions. Periodic boundary conditions were introduced to the system to restrain the finite size effects.

In the simplest way, spins of the Ising model can be considered as equivalent to the BOLD activity in the brain with +1 for the activity higher than the baseline activity and -1 for the activity lower than the baseline activity. The classical Ising model exhibits long range correlations at the critical temperature, which explains the observed interactions of the spins that are spatially distant from each other. This fact can be compared with the functional integration observed in the brain. The

brain maintains a balance between the functional integration and segregation in order to perform efficiently (Tononi et al., 1998; Sporns and Honey, 2006). As observed in the behaviour of the brain, there are separate regions which are specialized to perform certain functions. While functioning separately, these regions need to exchange information with each other in order to function as a complete system. This process is explained as the functional integration and can be compared with the long range correlations observed in the Ising model. Thus the classical Ising model was chosen to model the oscillations observed in BOLD signal for comparison.

References

- Brush SG (1967) History of the Lenz-Ising model. Reviews of modern physics 39(4):883
- Chialvo DR (2010) Emergent complex neural dynamics. Nature physics 6(10):744–750
- Das T, Abeyasinghe P, Crone J, Sosnowski A, Laureys S, Owen A, Soddu A (2014) Highlighting the structure-function relationship of the brain with the Ising model and graph theory. BioMed research international
- Landau DP, Binder K (2014) A guide to Monte Carlo simulations in statistical physics. Cambridge University Press
- Sporns O, Honey CJ (2006) Small worlds inside big brains. Proceedings of the National Academy of Sciences 103(51):19,219–19,220
- Tononi G, Edelman GM, Sporns O (1998) Complexity and coherency: integrating information in the brain. Trends in cognitive sciences 2(12):474–484

APPENDIX B: CRITICAL EXPONENTS AND SCALING RELATIONS

1

APPENDIX B: Critical exponents and scaling relations (Landau and Binder, 2014)

0.1 Critical exponents

Critical exponents of Magnetization, Susceptibility and Specific Heat was calculated by fitting Eq. 1 -5 for the respective plots. For Susceptibility and the Specific Heat, since there are two separate equations for fitting the right hand side and the left hand side of the plot, we obtained two critical exponents using both equations. Then the exponent that has the minimum error was chosen.

0.1.1 Magnetization

$$M(T) = P_1 \left[\frac{T_c - T}{T_c} \right]^\beta \quad (1)$$

0.1.2 Susceptibility

$$\chi_{left}(T) = P_1 \left[\frac{T_c - T}{T_c} \right]^{-\gamma} \quad (2)$$

$$\chi_{right}(T) = P_1 \left[\frac{T - T_c}{T_c} \right]^{-\gamma} \quad (3)$$

0.1.3 Specific Heat

$$c_{v-left}(T) = P_1 \left[-\ln \left(\frac{T_c - T}{T_c} \right) \right]^\alpha \quad (4)$$

$$c_{v-right}(T) = P_1 \left[-\ln \left(\frac{T - T_c}{T_c} \right) \right]^\alpha \quad (5)$$

0.1.4 Correlation Function

In order to calculate the correlation length (ξ) for different temperatures, Eq. 6 was fitted for the correlation function vs. distance plot at each temperature. At the critical temperature, the correlation length goes to infinity and Eq. 6 simplifies into Eq. 7. Furthermore, the correlation function at the critical temperature is said to behave according to Eq. 8 at the critical temperature (Witthauer and Dieterle, 2007). Therefore the critical exponent for the correlation function (η) was obtained by fitting Eq. 8 for the correlation function vs. temperature plot at the critical temperature. By plugging in

this value in the denominator of Eq. 7, we were able to calculate the dimensionality.

$$G(r) = \frac{\exp\left(-\frac{r}{\xi}\right)}{r^{d-2+\eta}} \quad (6)$$

$$G(r)[atT_c] = \frac{1}{r^{d-2+\eta}} \quad (7)$$

$$G(r)[atT_c] = P_1 (r)^{-\eta} \quad (8)$$

0.1.5 Correlation Length

Correlation lengths which have been calculated by fitting Eq. 6 was plotted as a function of temperature. Eq. 9 and 10 was used to fit the above mentioned plot from left hand side and the right hand side and ν , the critical exponent of the correlation length was obtained.

$$\xi_{left}(T) = P_1 \left[\frac{T_c - T}{T_c} \right]^{-\nu} \quad (9)$$

$$\xi_{right}(T) = P_1 \left[\frac{T - T_c}{T_c} \right]^{-\nu} \quad (10)$$

0.2 Scaling relations

Critical exponents calculated from the above mentioned methods obey the scaling relations presented in Eq. 11 - 13.

$$(2 - \eta) \nu = \gamma \quad (11)$$

$$\frac{\nu}{2} (\eta + d - 2) = \beta \quad (12)$$

$$2 - \nu d = \alpha \quad (13)$$

Variables and constants in the equations

P_1 - Constant

T - Temperature

T_c - Critical temperature

ξ - Correlation length

r - Distance

d - Dimensionality

Critical exponents:

β - Magnetization

γ - Susceptibility

α - Specific Heat

η - Correlation Function

ν - Correlation length

References

Landau DP, Binder K (2014) A guide to Monte Carlo simulations in statistical physics. Cambridge University Press

Witthauer L, Dieterle M (2007) The phase transition of the 2d-ising model

APPENDIX C: LABELS OF 84 PARCELLATIONS OF THE BRAIN

1

APPENDIX C: Labels of 84 parcellations of the Brain

<i>Right hemisphere</i>	<i>Left hemisphere</i>
1. Thalamus-Proper	43. bankssts
2. Caudate	44. caudalanteriorcingulate
3. Putamen	45. caudalmiddlefrontal
4. Pallidum	46. cuneus
5. Hippocampus	47. entorhinal
6. Amygdala	48. fusiform
7. Accumbens-area	49. inferiorparietal
8. bankssts	50. inferiortemporal
9. caudalanteriorcingulate	51. isthmuscingulate
10. caudalmiddlefrontal	52. lateraloccipital
11. cuneus	53. lateralorbitofrontal
12. entorhinal	54. lingual
13. fusiform	55. medialorbitofrontal
14. inferiorparietal	56. middletemporal
15. inferiortemporal	57. parahippocampal
16. isthmuscingulate	58. paracentral
17. lateraloccipital	59. parsopercularis
18. lateralorbitofrontal	60. parsorbitalis
19. lingual	61. parstriangularis
20. medialorbitofrontal	62. pericalcarine
21. middletemporal	63. postcentral
22. parahippocampal	64. posteriorcingulate
23. paracentral	65. precentral
24. parsopercularis	66. precuneus
25. parsorbitalis	67. rostralanteriorcingulate
26. parstriangularis	68. rostralmiddlefrontal
27. pericalcarine	69. superiorfrontal
28. postcentral	70. superiorparietal
29. posteriorcingulate	71. superiortemporal
30. precentral	72. supramarginal
31. precuneus	73. frontalpole
32. rostralanteriorcingulate	74. temporalpole
33. rostralmiddlefrontal	75. transversetemporal
34. superiorfrontal	76. insula
35. superiorparietal	77. Cerebellum-Cortex
36. superiortemporal	78. Thalamus-Proper
37. supramarginal	79. Caudate
38. frontalpole	80. Putamen
39. temporalpole	81. Pallidum
40. transversetemporal	82. Hippocampus
41. insula	83. Amygdala
42. Cerebellum-Cortex	84. Accumbens-area

APPENDIX D: DISTANCE CALCULATIONS, FURTHER STUDY OF THE DIFFERENCE IN T_c AND ADDITIONAL FIGURES

1

APPENDIX D

(I): Distance Calculations

Distance between the correlation distributions

To compare the correlation distributions, the distance between the correlation distributions were calculated using the Kolmogorov-Smirnov test (Young, 1977). The temperature (T_{min}) which minimizes this distance was obtained for the ten realizations separately and compared with T_c using a two-sample t-test (t-test results are discussed in the manuscript).

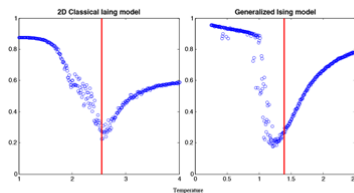


Fig. 1 Distance between the correlation distributions as a function of temperature for the 2D classical Ising model and the generalized Ising mode. Red vertical line corresponds to the critical temperature T_c .

References

Young, Ian T. "Proof without prejudice: use of the Kolmogorov-Smirnov test for the analysis of histograms from flow systems and other sources." *Journal of Histochemistry & Cytochemistry* 25.7 (1977): 935-941.

(II): Inter-subject variance of T_c and T_{min}

The work presented in the paper was performed using the average connectivity over 66 subjects. Variation of the critical temperature and T_{min} was due to simulating the 2D classical Ising model and the generalized Ising model ten times using the same average connectivity. However, we simulated the generalized Ising model using 66 different structural connectivity matrices and the figure below illustrates how T_c and T_{min} are distributed among the subjects.

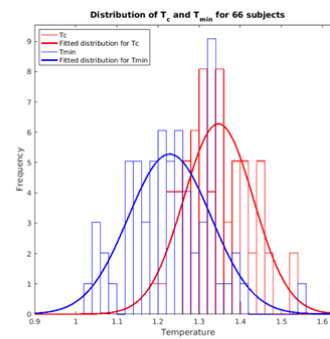


Fig. 2 Histograms of T_c and T_{min} together with the fitted distributions for the generalized Ising model for 66 subjects

(III): Further study of the difference in T_c

In order to investigate the observed difference of T_c for the generalized Ising model and the 2D classical Ising model we generated different connectivity matrices by gradually changing the sparsity of the matrices. Fig. 3 represents the initial structural connectivity which is been used for the generalized Ising model simulations and then how an intermediate structural connectivity as well as the structural connectivity of the 2D classical Ising model.

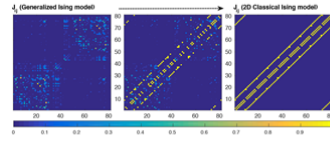


Fig. 3 Structural connectivity matrix of the generalized Ising model, an intermediate structural connectivity and the structural connectivity used for the 2D classical Ising model

Starting with the structural connectivity used in the generalized Ising model simulations and by changing/removing connections randomly preserving the randomness, the structural connectivity was gradually transformed to that of the 2D Ising model. The connectivity matrices build during this transformation were used in the generalized Ising model simulations and the critical temperature was obtained from each simulation. In Fig. 4, critical temperature is plotted as a function of the sparsity of the connectivity matrix. Transition is from the generalized Ising model with a sparsity of 0.06 to the 2D classical Ising model with a sparsity of 0.95. From this figure, it can be seen that the sparsity of the connectivity matrix could explain the difference observed

in the critical temperatures from the generalized Ising model and the 2D classical Ising model. However, the variations observed in the critical temperature in this figure could be due to the random procedure followed in order to get different connectivity matrices during the transition.

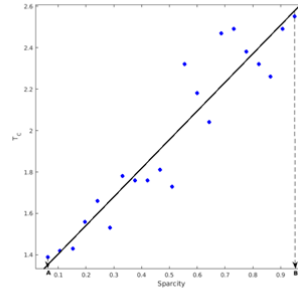


Fig. 4 Critical temperature versus sparsity of the connectivity matrices. Point A represents the sparsity of the generalized Ising model and point B the 2D classical Ising model

(IV): Global degree as a function of temperature

In graph theory, degree of a node is said to be the number of connection that node has. For a graph, the global degree gives the average degree of the whole network by taking the average over the number of nodes the network has. We have calculated the global degree for using the results of the simulations of 2D classical Ising model and the generalized Ising model as a function of temperature. From this plot, it is evident that the degree of the generalized Ising model maximizes at a temperature different from the critical temperature but similar to T_{\min} .

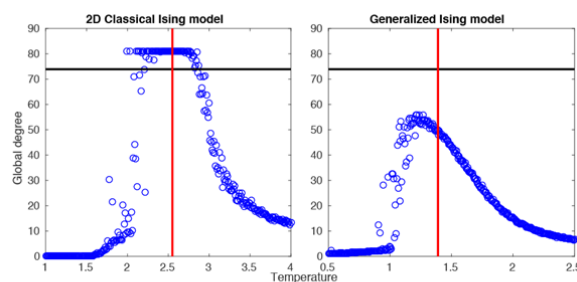


Fig. 5 Global degree as a function of temperature for the 2D classical Ising model and the Generalized Ising model. Black horizontal line represents the global degree for the empirical functional connectivity. Red vertical line represents the critical temperature for each case